ELSEVIER

Thermochimica Acta 333 (1999) 183–190

thermochimica acta

Electric field calibration in micro-electrode chambers by temperature measurements

Henning Glasser, Thomas Schnelle, Torsten Müller, Günter Fuhr*

Institut für Biologie, Humboldt-Universität zu Berlin, Lehrstuhl für Membranphysiologie, Invalidenstrasse 42, 10115 Berlin, Germany

Received 30 March 1999; received in revised form 26 April 1999; accepted 28 April 1999

Abstract

To study the effect of strong ac-fields (up to 100 kV/m at frequencies between 0.25 and 40 MHz), suspended or adherently growing animal cells were cultivated on micro-electrode structures. The use of miniaturised electrodes has the advantage that cells can be exposed to electric fields in physiological solutions of high conductivity. A disadvantage is that the actual field strength near a cell depends both on its location and on other parameters. The problem is that stray dielectric losses in and near the chamber change the electric field in an undefined, frequency dependent manner.

This paper compares three different techniques for estimating the field: (i) impedance measurements, (ii) the measurement of dielectrophoretic forces and (ii) a new calorimetric method within a test chamber. Advantages, limitations and possible applications are discussed.

Keywords: Thermometry; Heat production; Conductivity; High frequency electric field; Quadrupole levitation

1. Introduction

Nowadays, biological objects are often exposed to or manipulated by high frequency electrical fields [1–9]. To test the resulting stress we brought suspended cells directly onto miniaturised planar electrode systems [10–12]. Because heat is easily removed from miniaturised systems, cells may be cultivated at high field strength, even at physiologically relevant salt concentrations. Characterising field effects depend on a knowledge of the field in the vicinity of the cells. At high frequencies, the determination of the actual field strength is difficult. Stray capacitances and variable suspension conductivity make it difficult to calculate the actual field from the generator output.

For this reason the field strength at the position of interest has to be measured. Normally this is done by impedance measurements or by a determination of dielectrophoretic forces on small test particles (the forces are proportional to the gradient of the square of the local field strength). However, interpretation of impedance data requires knowledge of the electric characteristics of the investigated system, while dielectrophoretic techniques (electro-rotation and particle levitation [9,13–17]) are time consuming.

This paper introduces a method which uses the heat dissipation within the measuring chamber to measure the effective electric power supplied by the electrodes. Briefly, we assume that at low frequencies the only direct result of electric fields is the migration of ions.

*Corresponding author. Fax: +49-30-209-38635; e-mail: g.fuhr@webserv.biologie.hu-berlin.de

0040-6031/99/$ – see front matter
PII: S0040-6031(99)00100-8

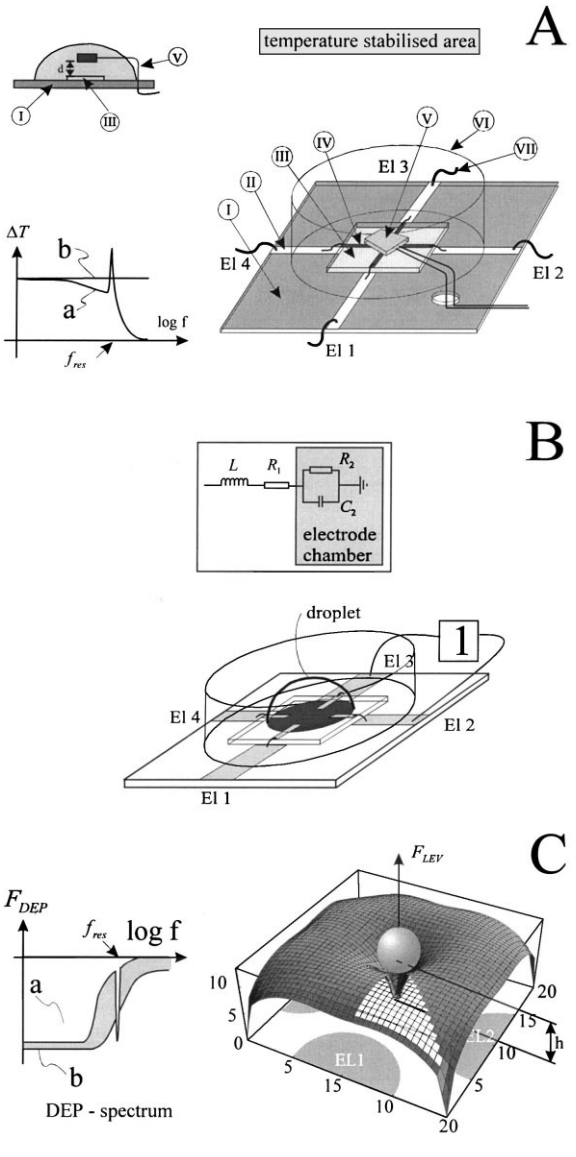

$$F_{DEP} = 2\,\pi\,\varepsilon_0\varepsilon_r R^3\,\mathrm{Re}\left[f_{CM}\right]\nabla(K\,E_{APP}^2) + O\,(R^5) = F_{LEV} = \frac{4}{3}\,\pi\,R^3\Delta\,\rho\,g$$

Fig. 1. Methods for determining the local field strength in miniaturised electrode chambers. (A) Calorimetric method: right part: schematic of an photolithographically processed electrode chip (III) placed on circuit board (I). The copper tracks (II) are connected with gold electrodes (IV) via bond wires of 25 μm thickness. The thermal resistor (V) is placed above the electrodes in free solution. The circle (VI) shows the glass ring of the media reservoir (max 4 ml). The electrode chamber is connected to the generator via BNC cables (VII). The small pictogram (left upper) shows a cross-section. The arrow (d) indicates the distance between electrodes and thermal resistor (about 250–500 μm). The chamber was thermostated at 37°C±0.05°C. To measure the heating we used a HP 34401A multimeter. Both curves in the small diagram represent the idealised (b) and the actual (a) behaviour of the temperature difference $\Delta T=(T-37°C)$. For the ideal curve we have assumed that no dielectric losses reduce the generator output; (B) the impedance method: to determine the impedance it is assumed that the electric properties of the chamber may be modelled by the RC-circuit given in the upper part for each electrode to a virtual ground; (C) the levitation method: here a test particle is placed between four cross-like electrodes (EL1, El2,..) that are driven by high frequent ac-fields. Due to induced surface charges the particle suffers a force (F_{LEV}). The latex spheres are centred between the electrodes, and simultaneously, lifted. In the shown "funnel-like" plane the dielectrophoretic force is counterbalanced by gravitation, hence a particle will rest on this plane at height h. The height h depends on the field frequency. In the left part a real curve (a) is compared with an ideal one (b). Again the later neglects dielectric losses.

This drift leads to a corresponding heat production. At steady state, the heat generation results in a temperature rise, which is taken as a reference. At higher frequencies the temperature rise will be different, due to dielectric losses arising, e.g., from reactive impedances, surface charges at the electrodes and other, less predictable effects.

2. Material and methods

Fig. 1 outlines the methods for detecting the strength of high frequency fields within miniaturised electrode systems. Our chamber (Fig. 1(A)) is made by a glass-chip with four small Au-electrodes (b: 50 μm, l: 4500 μm, h: 0.5 μm). This chip is mounted on a circuit board with four larger strip conductors (El1 through El4). The pairs El1/El2 and El3/El4 could each be terminated with a 50 Ω resistor (see Fig. 6(B)).

2.1. Temperature measurement

The system was thermostated at 37°C, the temperature, at which animal cells are usually cultivated. The medium temperature was stabilised with an accuracy of ±0.05°C. When the field is switched on, heat production increases the temperature inside the thermostated system. This temperature rise depends on the field strength and on the electric conductivity of the solution. This was illustrated for a homogeneously heated sphere of radius a where the time-averaged

heat generation per unit volume q is

$$q = \sigma^* E^2, \tag{1}$$

here E is the electric field strength. The balance between heat generation within the sphere and heat dissipation at its surface determines the temperature T, given by

$$T = T_0 + (a^2 q/2\chi). \tag{2}$$

Here σ in Eq. (1) represents the conductivity and χ the thermal conductivity of the fluid. T_0 is the ambient temperature of the sphere [18]. Therefore, T depends linearly on E^2 provided T_0, σ and χ are held constant (T is independent of the size of heated volume). Hence it is possible to use the temperature T as an indicator of E^2 which is, in turn, proportional to $\sigma^* U^2$. Here E and U are local quantities of the field strength and voltage, of course.

To measure the temperature within our system, a thermal resistor (KTY11-2A, Siemens, Germany, dimensions $2\times2\times1$ mm^3) was mounted 500 μm above the electrodes (marked by "V" in Fig. 1(A)). The connectors of the resistor were electrically isolated with epoxy resin (302-3, Polytek, USA), the temperature measured every 55 s. The fields were generated using a HP 8116A generator. Within temperature experiments the following parameters were varied:

1. applied amplitude (1 V<U_{APP}<4 V),
2. field frequency (500 kHz<f<40 MHz),
3. conductivity of the solution (0.1 S/m<σ<1.266 S/m) and
4. geometry of electrodes.

2.2. Impedance measurement

After the chamber was filled with 4 ml salt solution the impedance Z was determined with a HP 4194A network analyser (Hewlett-Packard, Germany) at the position indicated by "1" in Fig. 1(B) [19]. The determination of Z and the phase angle Φ is based on the equivalent circuit shown in the upper part of Fig. 1(B).

From Z and Φ the dissipated power P can be calculated:

$$P = \frac{U^2 * \cos\Phi}{|Z|}, \tag{3}$$

where U_{APP} is the voltage supplied by a generator.

Because impedance and the phase shift depend on the field frequency f, the power was registered between 100 kHz and 40 MHz. A further parameter that determines the impedance is the conductivity σ of the solution which was varied between 0.147 and 1.266 S/m.

2.3. Levitation measurements

As test particles we used latex beads (Standard Dow Latex, diameter 8, 15 and 20 μm, SERVA). For levitation experiments, the electrode chip was filled with 20 μl latex beads suspended in water. By adding KCl the conductivity of the suspension was adjusted to σ=27 mS/m. To levitate the particles we used a cross-like arrangement of four micro-electrodes which are driven by rectangular pulses (duty cycle 50%) supplied by a HP 8116A generator, for further details see [20].

Field-induced levitation is an effect that is caused by dielectrophoretic forces F_{DEP}. These forces depend on gradient of E^2 and higher derivatives of electric potential and also on electric relaxation processes at the surface of the particle. Hence the levitation depends on the field frequency. A detailed discussion [21,22] gives

$$\vec{F}_{DEP} = U_{rms}^2 \sum_{i=1}^{\infty} \vec{\alpha}_i(\vec{x}/a) * (R/a)^{2i+1} \tag{4}$$

with voltage U, particle radius R, co-ordinates x, multipole order i (i=1,2,... correspond to dipole, quadrupole,... order), and electrode distance a. In the functions α_i both dielectric properties and geometric properties (electrode design and drive) are summarised.

Due to the high permittivity of water, most biological cells and artificial particles like latex spheres are repelled from regions of high field strength (electrodes), at least at high field frequencies. The cross-like symmetry of the chamber centres and lifts the particles. The height of levitation was measured as a function of the applied field strength and field frequency (actuator type: MT 12, Heidenhain GmbH, Traunreut, Germany):

1. by lifting of a sedimentated particle using F_{DEP} and

2. detection of the levitation height of a sedimenting particle.

The distance (h, Fig. 1(C)) between the plane of electrodes and the equatorial line of the bead was assessed. The height measurement and focus control is described in more detail in Ref. [20]. The standard deviation of these measurements was about $\pm 2\,\mu m$.

3. Results

3.1. Particle levitation

Fig. 2(A) shows a contour plot of E^2; the field was numerically calculated for the real geometry of the electrode chamber. Because under our experimental conditions latex particles experience negative dielectric forces ($F \sim -\nabla E^2$), they are repelled from the electrodes and centred. Due to symmetry, there is no electric field on the central vertical axis and levitation is caused by higher moments (see Eq. (4)). The height which a latex particle reaches is given by a balance between the force lifting it and sedimentation. A theoretical height can be calculated in quadrupole approximation. Fig. 2(B) shows how this height corresponds to measurements: Only for large particles (20 μm) and small amplitudes (0 V<U<5.5 V) are the measured levitation data in accordance with the expected ones. At higher voltages the increased heat production (proportional to U^2) leads to thermoconvection. This results in significant deviations between measured and expected curves. Since quadrupole forces scale as R^5 (see Eq. (4)) small particles need higher voltages to reach a certain height.

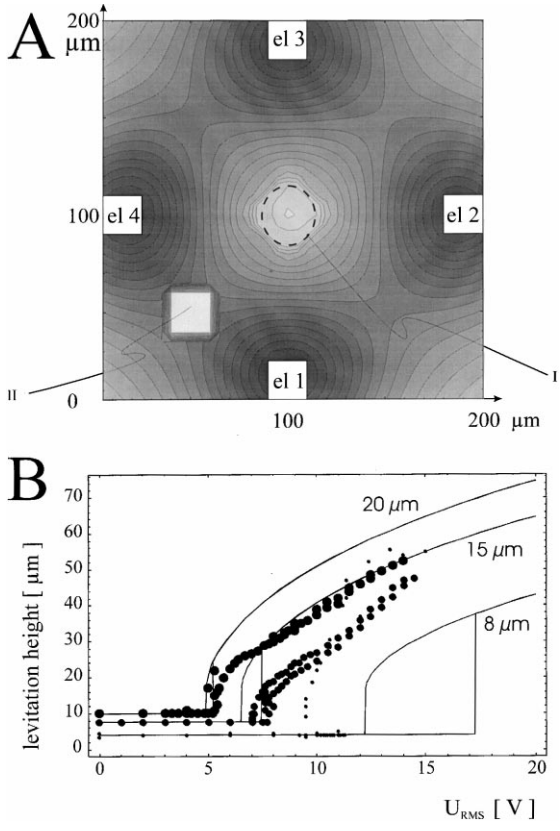

Fig. 2. (A) Contour plot of the time average of E^2. Darker areas mark regions of higher field strength. The latex sphere (dashed line circle) senses the field strength at the centre of the chamber (I). A sensor (II) placed near the electrodes would deform the field to an unacceptable degree; (B) levitation height of latex beads (conductivity of the suspension σ=27 mS/m) measured as a function of the applied voltage U_{RMS}. For the measurement we used a chamber with four-electrodes spaced at 41.6 μm. The theoretical curves (straight lines) are calculated according Eq. (4) up to quadrupole order, the parameter is particle size.

3.2. Field determination by temperature and impedance measurements

In Fig. 3 the results of typical impedance measurements are given. Fig. 3(A) shows how the power factor cos $\Phi/|Z|$ from Eq. (3) depends on the field frequency; the parameter of the curves (a)–(d) is the conductivity of the solution. Due to dielectric losses the power factor starts to decrease at a field frequency of about 10 MHz. Fig. 3(B) is obtained from Fig. 3(A), it shows how the power factor at a given frequency changes with the conductivity of the solution.

Fig. 4(A) characterises the temperature measurement and Fig. 4(B) confirms the validity of Eqs. (1) and (2). Furthermore, according to Eqs. (1) and (2) the linearity between ΔT and U^2 should be independent of the waveform, the conductivity of the solution and the scaling of electrode system. The results shown in Fig. 5(A)–(C) confirm these aspects; linearity is ensured up to 40 MHz. The dotted curve in Fig. 5(C) was taken at the comparatively low frequency of 500 kHz. Because dielectric losses at this frequency can be neglected, we use this curve as a reference, assuming that all power supplied by the generator

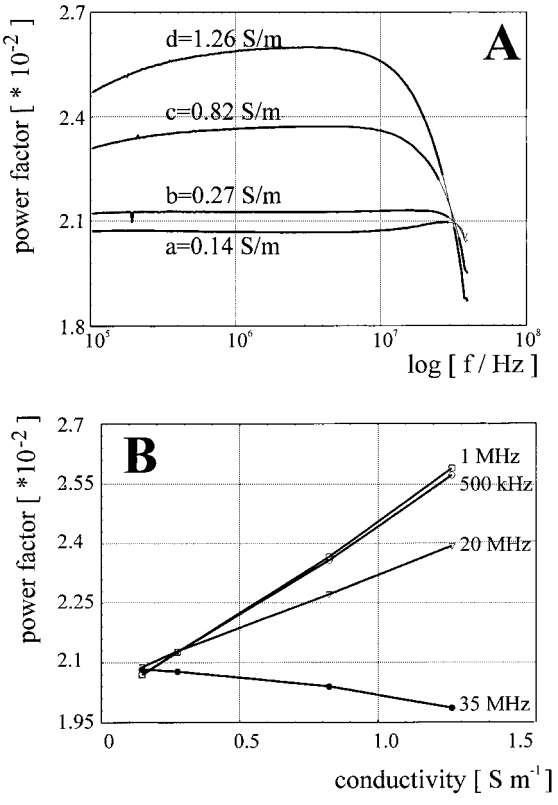

Fig. 3. (A) The power factor as a function of the field frequency, measured in a micro-electrode chamber with 200 μm spaced electrodes. The parameter is the conductivity of the solution. The used BNC cable (40 cm length) was terminated with 50 Ω; (B) power factor at constant frequencies by different solution conductivities (re-scaled from picture A).

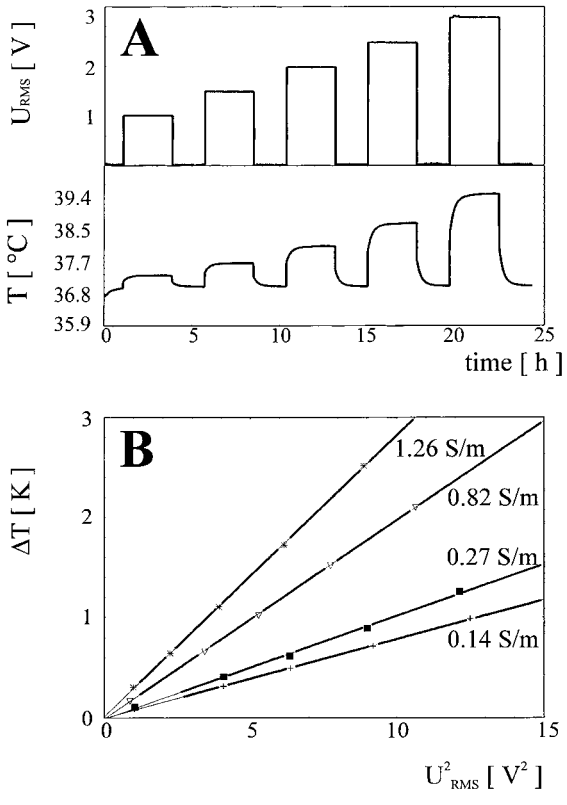

Fig. 4. (A) Correlation between the generator output (U_{RMS}, f=500 kHz) and the temperature of the solution. The data were measured in an electrode chamber (122 μm distance) installed in a 37°C thermostated water bath. The solution conductivity was σ=1.266 S/m. The typical field exposure time is about 3 h, the field switch off time to thermal re-calibration of the measurement system is set about at 2 h; (B) dependency of the temperature change (ΔT) on conductivity and applied square amplitude. All curves were measured at a constant frequency (500 kHz).

reaches the solution above the electrodes. Defining a efficiency ratio $K = \sqrt{U^2_{local}/U^2_{applied}}$, the dotted, "500 kHz"-curve would represent a K-value of 1 and the "20 MHz"-curve (σ=1.26 S/m) a K-value of 0.6.

Fig. 6(A) compares the results of an impedance measurement (curve (a)) with that of a temperature measurement (curve (b)). Both the shown power factor ($\cos \Phi/|Z|$) and $\Delta T=(T-37^{\circ}C)$ should be proportional to U^2(see Eqs. (1)–(3)), and therefore, the ratio $P/\Delta T$ is independent of the field frequency.

The interpretation of measured impedance data requires knowledge about the electric characteristics of the chamber. As our system is fluid filled and contains metal electrodes, its actual equivalent circuit should be different from the simple RC-circuit shown in Fig. 1(A). However, the exact determination of an adequate equivalent circuit is a time consuming and difficult task that includes the solution of nonlinear equation systems [23].

An additional aspect concerns the impedance of the conducting cables. To predict dielectric losses the conductors should be terminated with 50 Ω. This demand is hardly practicable because it includes the small Au-electrodes and the variable conductivities of the fluid. A first approach is the integration of 50 Ω resistors at the electrode strips on the circuit board. Furthermore, the inductances L were added to com-

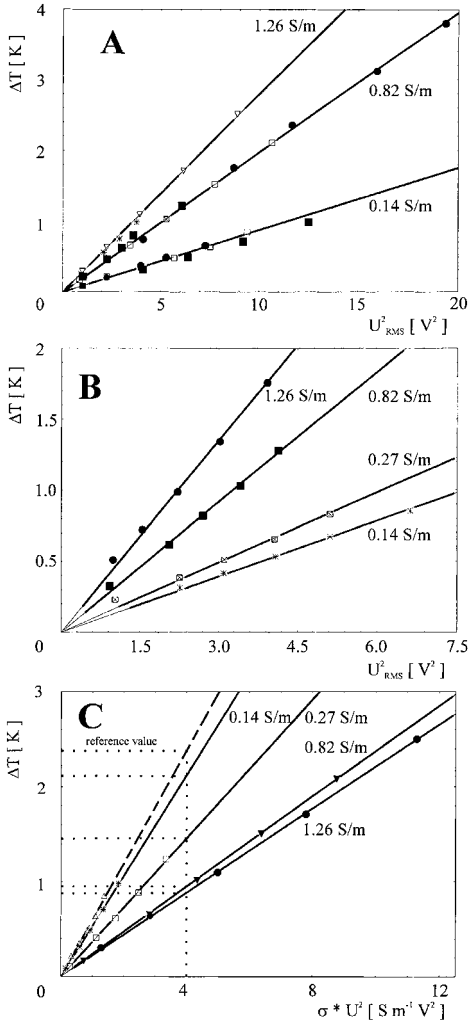

Fig. 5. Dependence of ΔT on signal form, electrode geometry and field frequency. To test the influence of the chamber geometry we used three chambers A, B and C with electrode distances of 41.6, 122 and 200 μm, respectively. (A) Temperature changes as a function of U^2 measured at a frequency of 500 kHz and different conductivities with different chambers (□: chamber type A; ■: chamber type B; ●: chamber type C). The dependence of ΔT on the signal form (*: sinusoidal, ▽: rectangular) was studied at σ=1.266 S/m with chamber type B; (B) temperature changes as a function of U^2 measured at a frequency of 40 MHz and different conductivities with chamber A; (C) temperature changes as a function of U^2 measured at a frequency of 20 MHz and different conductivities with chamber A (straight lines). The dashed curve represents a 500 kHz measurement for a σ=0.1 S/m solution. This curve is taken as a reference because at 500 kHz dielectric losses can be neglected, i.e. it is assumed that $U_{APP}=U_{ACT}$ (100% of the applied field is acting). The ratio $\Delta T_{(U_{APP},f)}/\Delta T_{REF}$ represents an efficiency, given by $\sigma * U^2_{ACT}/\sigma * U^2_{APP}$.

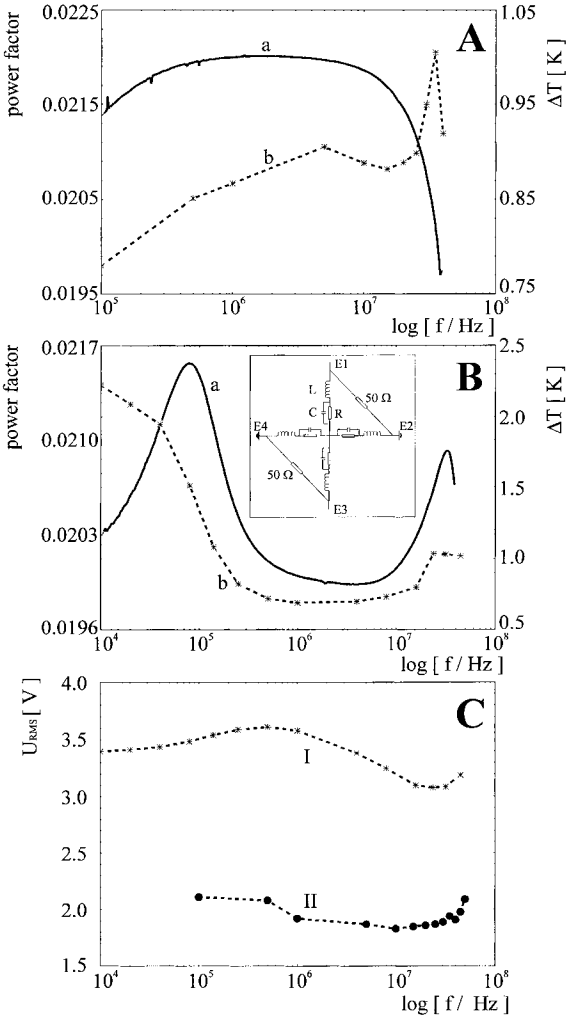

Fig. 6. Comparison between temperature, applied amplitude and impedance as a function of the frequency at 37°C; (A) curve (a) displays the power factor ($\cos \Phi/|Z|$) measured in a liquid filled chamber (σ=1.266 S/m; electrode distance=122 μm; left scale) which was connected to the generator with a BNC cable of 40 cm length. The heating (b) is scaled on the right side of diagram; (B) the same electrode chamber as in (A), which is adjusted to a resonance frequency at about 100 kHz by using an inductance (L) of 1 mH between each electrode and the BNC cable (electric details are shown in the electric network in the inset pictogram). The power factor curve (a) is plotted against frequency and scaled on the left side. The temperature curve (b) is scaled on the right side; (C) curve (I) shows the generator output amplitude recorded in parallel to the temperature measurement in (A). The generator amplitude was set to 3.5 V_{RMS}. Curve (II) represents the generator amplitude output during temperature measurements of (B) (amplitude: 2 V_{RMS}).

pensate the electrode capacities (denoted by C) [24]. This gave a better proportionality between the measured power factor and the measured temperature rise (Fig. 6(B)).

Fig. 6(C) shows the generator signal as it reaches the position ''1'' shown in Fig. 1(A). The curves I and II represent the signals used for the curves 6A (b) and 6B (b), respectively.

In an aqueous solution with σ=1.266 S/m (comparable to the conductivity of a physiological culture medium) and applied field frequency f=500 kHz, the temperature data indicate a field factor of K=0.707 (an acting field strength E_{ACT}=0.707*E_{APP}).

4. Discussion

High frequency electric studies on biological cells need detailed information about the local field strength. This paper compares three different techniques for estimating the field: (i) impedance measurements, (ii) the measurement of dielectrophoretic forces and (iii) a new calorimetric method. None of these techniques sense the local field strength directly, but all determine a quantity that is proportional to the time average of E^2. This is valid for the impedance based power P, the levitation height h and for field induced heating ΔT.

Apart from being expensive, the sophisticated impedance method requires additional knowledge about the electric network of the tested system. This information is not easy to obtain [8]. The levitation method is time consuming and sensitive to thermoconvection which limits its applicability. Contrastingly, the ΔT-method is simple and the relation between ΔT and U^2 is linear up to 40 MHz. The position of thermosensor is not critical and the sensor can be placed far enough from the electrodes to minimise interactions. We have used a distance of ca. 500 μm. Closer, the sensor could deform the field in an unacceptable manner (see Fig. 2(A), ''II'').

Besides using the thermometric method to monitor the local electric field, there is an useful side effect. The temperature can be used to optimise the cultivation conditions – especially under the action of high frequency fields. The method gives an alternative to the temperature dependent fluorescence shift of dye-labelled phospholipid vesicles to visualise small local temperature changes [25].

The thermometric method represents an alternative tool for quantifying field-mediated effects on living cells in physiological media and can assist the interpretation of data in e.g. electro-fusion, electro-poration, long time field application and studies of field influences on cell membrane transport processes.

Acknowledgements

We acknowledge the Fraunhofer Institute for Silicium Technology (ISiT, Itzehoe) for fabrication the micro-electrode structures. We thank Dr. J. Gimsa and D. Wachner for using the impedance analyser. We would like to thank Dr. S.G. Shirley and Dr. R. Hagendorn for stimulating discussions and critical reading of the paper. This work was granted by the ''Forschungsgemeinschaft Funk'', grant no.: 5985.

References

[1] J.H. Bernhard, Phys. Med. Biol. 37 (1992) 807.
[2] G. Fuhr, U. Zimmermann, S.G. Shirley, in: U. Zimmermann, G.A. Neil (Eds.), Electromanipulation of Cells, Cell motion in time varying fields: Principles and potential, CRC Press, Boca Raton, 1996, p. 259.
[3] V.L. Sukhorukov, H. Mussauer, U. Zimmermann, J. Membr. Biol. 163 (1998) 235.
[4] F.F. Becker, X.-B. Wang, Y. Huang, R. Pethig, J. Vykoukal, P.R.C. Gascoyne, Proc. Natl. Acad. Sci. USA 92 (1995) 860.
[5] G. Fuhr, Th. Schnelle, T. Müller, H. Glasser, Th. Lisec, B. Wagner, Sensors and Actuators 7 (1995) 131.
[6] L.B. Margolis, S.V. Popov, Bioelectrochem. Bioenergetics 20 (1988) 143.
[7] H.P. Pohl, Dielectrophoresis, Cambridge University Press, New York, 1978.
[8] J. Gimsa, T. Müller, Th. Schnelle, G. Fuhr, Biophys. J. 71 (1996) 495.
[9] K.V.I.S. Kaler, T.B. Jones, Biophys. J. 57 (1990) 173.
[10] G. Fuhr, T. Müller, Th. Schnelle, R. Hagedorn, A. Voigt, S. Fiedler, M. Arnold, U. Zimmermann, B. Wagner, A. Heuberger, Naturwissenschaften 81 (1994) 528.
[11] G. Fuhr, H. Glasser, T. Müller, Th. Schnelle, BBA 1201 (1994) 353.
[12] H. Glasser, G. Fuhr, BBE 47 (1998) 301.
[13] Y. Huang, R. Hölzel, R. Pethig, X.-B. Wang, Phys. Med. Biol. 37 (1992) 1499.
[14] G. Fuhr, R. Hagedorn, in: P.T. Lynch, M.R. Davey (Eds.), Electrical Manipulation of Cells, Cell rotation, Chapman & Hall, London, 1996, p. 37.
[15] V.L. Sukhorukov, U. Zimmermann, J. Membr. Biol. 153 (1996) 161.
[16] W.M. Arnold, U. Zimmermann, J. Electrostatics 21 (1988) 151.

[17] G. Fuhr, Th. Schnelle, T. Müller, H. Hitzler, S. Monajembashi, K.O. Greulich, Appl. Phys. 67 (1998) 385.
[18] G. Fuhr, Th. Schnelle, R. Hagedorn, S.G. Shirley, Cell. Eng. Molecular Eng. 1 (1995) 47.
[19] J. Gimsa, D. Wachner, Biophys. J. 75 (1998) 1107.
[20] G. Fuhr, W.M. Arnold, R. Hagedorn, T. Müller, W. Benecke, B. Wagner, BBA 1108 (1992) 215.
[21] Th. Schnelle, T. Müller, S. Fiedler, G. Fuhr, J. Electrostatics 46 (1998) 13.
[22] T.B. Jones, Electromechanics of particles, Cambridge University press, Cambridge, 1995.
[23] J.Z. Bao, C. Davis, R.E. Schmuckler, IEEE Transactions on Biomed. Eng. 40 (1991) 364.
[24] T. Müller, J. Gimsa, B. Wagner, G. Fuhr, Microsystem Technol. 3 (1997) 168.
[25] Y. Liu, D.K. Cheng, G.J. Sonek, M.W. Berns, B.J. Tromberg, Appl. Phys. Lett. 65 (1994) 919.